

# Using Excimeric Fluorescence to Study How the Cooling Rate Determines the Behavior of Naphthalenes in Freeze-Concentrated Solutions: Vitrification and Crystallization

Gabriela Ondrušková, Lukáš Veselý, Jan Zezula, Johannes Bachler, Thomas Loerting, and Dominik Heger\*

Cite This: *J. Phys. Chem. B* 2020, 124, 10556–10566

Read Online

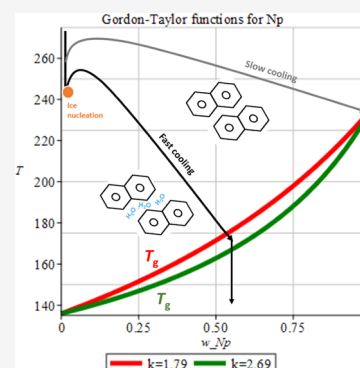
ACCESS |

Metrics & More

Article Recommendations

Supporting Information

**ABSTRACT:** We utilized fluorescence spectroscopy to learn about the molecular arrangement of naphthalene (Np) and 1-methylnaphthalene (MeNp) in frozen aqueous solutions. The freezing induces pronounced compound aggregation in the freeze-concentrated solution (FCS) in between the ice grains. The fluorescence spectroscopy revealed prevalent formation of a vitrified solution and minor crystallization of aromatic compounds. The FCS is shown as a specific environment, differing significantly from not only the pure compounds but also the ice surfaces. The results indicate marked disparity between the behavior of the Np and the MeNp; the cooling rate has a major impact on the former but not on the latter. The spectrum of the Np solution frozen at a faster cooling rate (ca 20 K/min) exhibited a temperature-dependent spectral behavior, whereas the spectrum of the solution frozen at a slower rate (ca 2 K/min) did not alter before melting. We interpret the observation through considering the varied composition of the FCS: Fast freezing leads to a higher water content expressed by the plasticizing effect, allowing molecular rearrangement, while slow cooling produces a more concentrated and drier environment. The experiments were conceived as generalizable for environmentally relevant pollutants and human-made freezing.



## INTRODUCTION

Ice and snow are important reaction media capable of accumulating various types of impurities.<sup>1,2</sup> The impurities, ubiquitously present in the atmosphere in the form of organic aerosols,<sup>3–5</sup> originate from various natural and anthropogenic sources, for example, sea salt, dust, and pollution.<sup>6,7</sup> The organic aerosols are formed *in situ* via chemical degradation, out of biological sources, or through deposition from atmospheric gases.<sup>8,9</sup> In the wider context, the physical and chemical properties of organic compounds found in environmental ices<sup>10</sup> can influence not only atmospheric and biochemical cycles<sup>11</sup> but also the ice nucleation ability of aerosol particles.<sup>12,13</sup> The relatively high concentrations of some pollutants deposited in the ices of the Arctic and the Antarctic and high-altitude mountains are explained by global distillation, also known as the grasshopper effect; this term denotes the process of long-range substance transport from warmer to colder areas.<sup>14–16</sup>

It is suggested that the chemical and photochemical reactivity of the compounds differs depending on their particular locations and physical states in or on the ice, with the relevant questions being whether the pollutants are present on the external surfaces of or between the ice crystals (the internal surfaces and veins or triple junctions) and whether they are dissolved, crystallized, or amorphous.<sup>2,17–22</sup> The micro- and macrostructure of the ice containing impurities is

influenced by various factors, including the phases from which the ice nucleates and grows (vapor or liquid),<sup>23</sup> pressure,<sup>24</sup> and freezing temperature.<sup>25,26</sup> Furthermore, it has been demonstrated<sup>27–30</sup> that the extent of the solute aggregation occurring during freezing depends on the cooling rate; for instance, Heger *et al.* observed a concentration increase by 3 and not less than 6 orders of magnitude in the fast and slow cooling, respectively, utilizing the methylene blue indicator.<sup>28</sup> The freeze-concentrated solution (FCS) is often located in between the ice crystals in the network of veins,<sup>26,30–34</sup> and it embodies a fundamental part of the heterogeneous ice matrix, in which the chemical reactivity is the highest. Despite the evidence that the cooling rate has a significant impact on the resulting meso- and macrostructure of ices and solutes, systematic studies are lacking.<sup>19,28,35–38</sup>

Aromatic hydrocarbons (AHs) range among those environmental pollutants that mostly originate from burning, such as that occurring in natural forest fires, or anthropogenic

Received: August 27, 2020  
Revised: October 22, 2020  
Published: November 6, 2020



processes.<sup>39</sup> AHs are present in air,<sup>40</sup> water,<sup>41</sup> soil,<sup>42</sup> and also space;<sup>43</sup> they absorb UV–Vis light depending on their structures and environment.<sup>11,44,45</sup> The simplest AHs are benzene,<sup>46</sup> naphthalene,<sup>47,48</sup> 1-methylnaphthalene,<sup>49</sup> and anthracene.<sup>50</sup> Each of these compounds exhibits characteristic luminescence spectra in various phases and is therefore well suited for speciation analysis, that is, finding the microscopic state of the compound, whether dissolved, crystallized, or amorphous. Naphthalene was studied as a proxy for secondary organic aerosols,<sup>51,52</sup> where its oxidation proves to be one of the key factors in environmental pollution.<sup>53</sup>

It is well established that fast cooling, high solute concentrations, and confinement supply the conditions for preferential vitrification over the crystallization of solutions, that is, the entire sample turns homogeneously into a glassy state. The very fast cooling rate of  $10^7$  K/s, denoted as hyperquenching, suffices for the full vitrification of even pure water.<sup>54</sup> In solutions, highly concentrated ones in particular, the cooling rate can be markedly reduced but still produces a fully vitrified sample.<sup>55</sup> Nanoconfinement is another strategy to deliver full vitrification, as proved in the micro-sized droplets,<sup>56</sup> the channels of minerals,<sup>57,58</sup> and the FCS veins within ice.<sup>19,30,36</sup> The last-mentioned case occurs when the solute concentration and cooling rate are insufficient for bulk vitrification. At such an instance, pure ice starts to crystallize, expelling most of the solutes to the ice surfaces. The freeze concentration process leads to phase separation of the pure ice and the FCS; the eventual fate of this stage depends on a number of factors and has not been fully understood to date, even though guided industrial and laboratory freezing would bring multiple advantages. When thermodynamically controlled, the FCS should reach the eutectic composition to crystallize; however, the FCS often vitrifies at concentrations higher than the eutectic composition because of kinetically controlled processes, such as supercooling. These effects are of high relevance for “pharmaceutical” freezing<sup>20,36,59–61</sup> and occur also in microemulsions that are considered proxies for aerosols.<sup>62</sup> The glass transition temperature of the bulk ( $T_g$ ) is distinguished from the glass transition temperature of the FCS ( $T_g'$ ) to stress the differences in the volume, composition, and preparation method.<sup>63</sup>

Here, we use fluorescence spectrometry and differential scanning calorimetry (DSC) on naphthalene (Np) and 1-methylnaphthalene (MeNp) as the model substances to deepen the understanding of the behavior and fate of the organic compounds on ice crystal boundaries and to describe the speciation of the compounds under various cooling conditions.

## EXPERIMENTAL PART

The resublimed naphthalene (Np) and the liquid 1-methylnaphthalene with the purity of 96% were purchased from Lachema (MeNp) and Alfa Aesar, respectively, and applied as received. A saturated Np solution was prepared by dissolving 3 mg of the Np in 200 mL of deionized water. The solubility of Np is 17.3 mg/L, which corresponds to  $1.35 \times 10^{-4}$  mol/L at 5 °C.<sup>64</sup> An oversaturated MeNp solution was obtained by mixing 60 mg of the pure MeNp and 200 mL of deionized water. The solubility of MeNp equals 24.7 mg/L, corresponding to  $1.74 \times 10^{-4}$  mol/L at 4 °C.<sup>65</sup> The solutions were placed into an ultrasonic bath, left there for approximately 8 h, and then filtered (filtering paper 2R/80); the resulting solutions used for freezing were verified by

measuring the absorption spectra at 20 °C and found to approach saturation. Aliquots of the solutions and the pure liquid MeNp were frozen using two methods: In the fast-cooled samples, we immersed the round quartz test tubes (inner diameter  $\sim 0.6$  cm) containing the solutions in liquid nitrogen ( $T = 77$  K); the average rate of cooling from 300 to 77 K was estimated to be  $(5.6 \pm 0.1)$  K/s. In the range of 273–136 K, where the freezing and/or vitrification occurs, the cooling rate is higher than the above-indicated one, probably about 20 K/s. The slow-cooled solutions were prepared by cooling in a freezer at 253 K, except the pure MeNp, which was tempered at 274 K and gradually cooled down to 77 K. The cooling rate is estimated to be in the order of 2 K/min for the freezer cooling. After the freezing, each sample was inserted into a precooled optical cryostat (77 K for the fast cooling and 253 K for the slow cooling, with the exception of the pure MeNp).

The microscopic Np crystals were prepared from a naphthalene solution of methanol *via* solvent evaporation on a microscope slide. We optimized the crystal thickness by setting the initial concentration such that the fluorescence self-absorption in the emission spectra could be avoided. Procedurally, high initial concentrations yielded thicker crystals with more pronounced self-absorption, while low ones did not enable us to observe a luminescence signal (possibly due to the Np evaporating or sublimating).

The fluorescence spectra were measured using an FLS 920 fluorescence spectrometer (Edinburgh Instruments) equipped with a 450 W Xe lamp as the light source, a PMT detector, and double-grating monochromators. The measurements were performed with front-face geometry in the quartz tubes, utilizing an Optistat DN2 cryostat (Edinburgh Instruments). After reaching the set temperature, the samples were kept at that level for 30 min prior to the measurement of each emission spectrum. All of the fluorescence emission spectra were obtained by excitation at  $\lambda_{\text{exc}} = 274$  nm.

Subsequently, we carried out differential scanning calorimetry (DSC) measurements, utilizing a PerkinElmer DSC 8000 calorimeter. Before the procedures, the solution (or the pure liquid MeNp) had been weighed in aluminum 50  $\mu$ L DSC crucibles. The actual cooling and heating rates are indicated for the individual thermograms; the ordinates are shown with the exothermic events oriented downward. The baseline correction was performed by subtracting a straight line from the scan to correct the sloping.

## RESULTS

**Naphthalene Crystals.** The microscopic-sized Np crystals at room temperature (melting point 353 K<sup>66</sup>) exhibit a fluorescence emission spectrum with several maxima between 315 and 360 nm (the red pattern in Figures 1 and S1–S3). The spectrum of the Np microcrystals at room temperature is slightly different from that of the Np solution (the black pattern in Figure 1) because of the self-absorption on the blue edge of the crystals' spectrum. The larger the sample's absorbance, the larger the self-absorption effect; thus, the fluorescence spectrum retreats at the left edge gradually in crystals having an increasing thickness, as shown in Figure S1, in accordance with the literature.<sup>48,67,68</sup>

The Np crystals exhibit spectra composed of multiple vibrationally resolved sharp peaks, which further separate with decreasing temperature; this is demonstrated in Figures S2 and S3 for the thin crystals prepared by methanol evaporation and

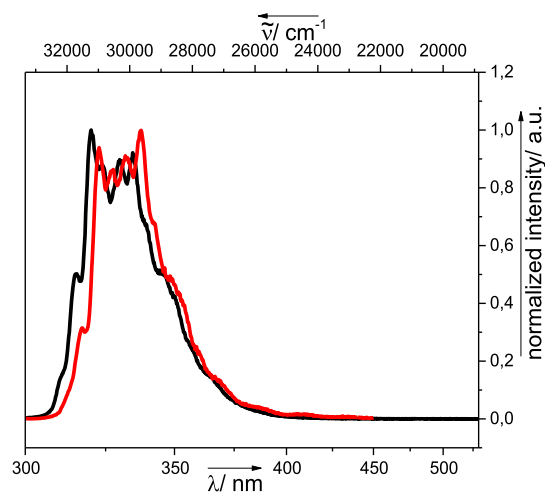


**Figure 1.** The normalized fluorescence emission spectra measured at room temperature: the Np aqueous solution (black line) and the Np microcrystals in a thin film on glass (red line).

in Figure S4 for the macroscopic-sized crystals. Such a spectral behavior is in accordance with previous observations by Márquez, *et al.*<sup>69</sup> The fluorescence emission of the Np crystals and Np aqueous solution typically steeply rises at 315 nm (0–0 emission band), exhibits characteristic vibrationally resolved bands (crystals: 322, 327, 330, 336 (max), 342, 345, 349, and 353 nm; solution: 320, 323, 330, and 334 nm), and gradually decreases at approximately 360 nm.<sup>47,48</sup>

**Naphthalene Frozen Solution.** The fluorescence emission spectra of the fast-cooled Np solution are shown in Figure 2 at two temperatures. At 77 K, the sample exhibits emission

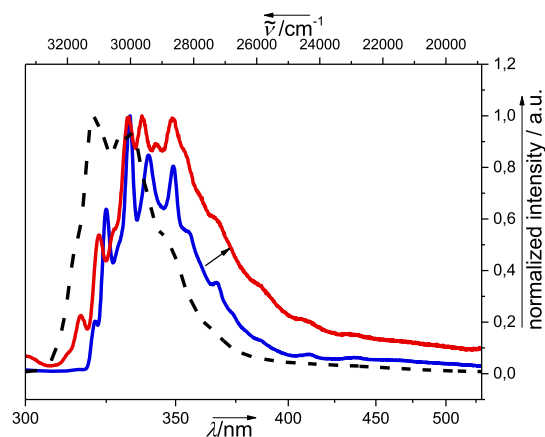


**Figure 2.** The normalized fluorescence emission spectra of the fast-cooled Np aqueous solution: 77 K (solid blue line) and 253 K (solid red line), and the spectrum of the unfrozen solution at 275 K (black dashed line). The arrow indicates the temperature-dependent broadening of the spectra.

with a maximum at  $\lambda_{em} = 333$  nm (the blue line). Upon increasing the temperature, a broadening is visible on both sides of the normalized emission spectra. On the red side of the spectrum, approximately in the region of 350–375 nm (indicated with an arrow in Figure 2 and also represented in Figure S5), the broadening is found to be a function of temperature: The signal increases with rising temperature and drops to the original intensity when the value lowers. We performed three temperature cycles to establish that the shapes

of the spectra predominantly depend on the temperature, without significant hysteresis (Figure S5C,D). The sample was further tempered in a freezer at 253 K for one week, with no significant spectral changes observed (Figure S5D). In the fast-cooled solution, the part of the spectrum above 350 nm remains almost constant below 150 K.

In an independent experiment, given the temperature of 77 K, an emission signal of anthracene at 411 and 436 nm was noted in addition to the Np signals. Anthracene is a well-known resistant Np impurity that complicates the luminescence spectrum through energy transfer.<sup>47,50,70</sup> The fluorescence signal of anthracene was notable only after the first freezing (the blue line in Figure S5D). Surprisingly, the anthracene signals vanished after the sample had been heated to 253 K and did not appear when the sample was further cooled down or during the temperature cycling.

The left-hand side of the spectra (below approximately 340 nm) indicates the presence of Np crystals in the frozen solution; this is best seen by comparing the spectra of the cooled solutions with those relating to the thin micron-sized crystals prepared by evaporating the methanol from the solution on the glass (Figure S3). The method is known to produce micron-sized crystals.<sup>68</sup> As the emission spectra depend on the crystals' thickness and temperature, they do not agree completely. Nevertheless, the band at 315 nm is sufficiently indicative, being present at 253 K but absent at 77 K for both the crystals and the frozen solutions; the effect is obvious from comparing the spectra of the frozen solutions with those of the thin crystals at identical temperatures (Figures S3).

The emission spectra of the slowly cooled Np solutions resemble to a large extent those of the fast-cooled solutions measured at 77 K (Figure 3). However, the spectra differ in

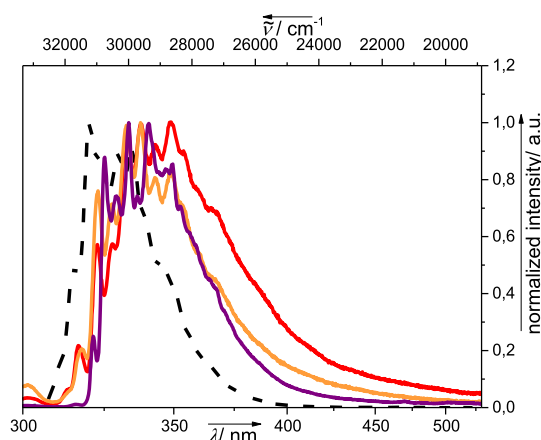


**Figure 3.** The normalized fluorescence emission spectra of the Np aqueous solution at 253 K after slow (orange line) and fast freezing (red line) and at 77 K after fast freezing (violet line), and the spectrum of the liquid solution at 300 K (black dashed line).

their thermal behavior: We do not observe major broadening on the red edges (Figure S6). Thus, at any temperature, the slowly cooled frozen samples are similar to the fast-cooled ones evaluated at 77 K, where the spectral band of the fast-cooled samples appears to be slightly narrower (Figure 3). The differences in the Nps' spectral behavior under the distinct cooling rates are of key importance and will be explained in the Discussion via references to various amounts of water in the vitrified portion of the FCS.

The DSC thermogram of the Np solution was measured at temperatures between 318 K (45 °C) and 93 K (−180 °C), with the rates of 50 and 30 K/min for the cooling (Figure S7, blue line) and the heating (Figure S7, red line), respectively. As expected, the most important features in the thermogram are the crystallization exotherm at  $t = -11$  °C ( $T = 262$  K, blue line) and melting endotherm at  $t = 2$  °C ( $T = 275$  K, red line). Besides these features associated with the bulk solution, we reproducibly observe the thermal events in the range from −30 to −100 °C, presumably related to the freeze-concentrated solutions. The most notable features are the endotherms that appear at −50 °C upon both the cooling and the heating. However, these signals are weak, and we do not employ them to interpret our observations.

**Pure 1-Methylnaphthalene.** In contrast to the Np, the pure MeNp is a liquid at room temperature (the literature values of the melting point agree on  $T = 242$  K<sup>66,71</sup>). We performed a DSC measurement on the sample of the pure MeNp (Figure S8). The cooling thermogram indicates an exotherm corresponding to the crystallization of the super-cooled MeNp. The melting endotherm at 30 K/min (Figure S8B) shows an onset at  $t = (-37.4 \pm 0.1)$  °C [ $T = (235.8 \pm 0.1)$  K]; such a value differs by 6 K from the results published thus far, probably because of the various purities used by other groups.

The pure MeNp at room temperature exhibits emission spectra comprising one main broad unresolved band with the maximum at 400 nm (Figure 4, red line). This characteristic is

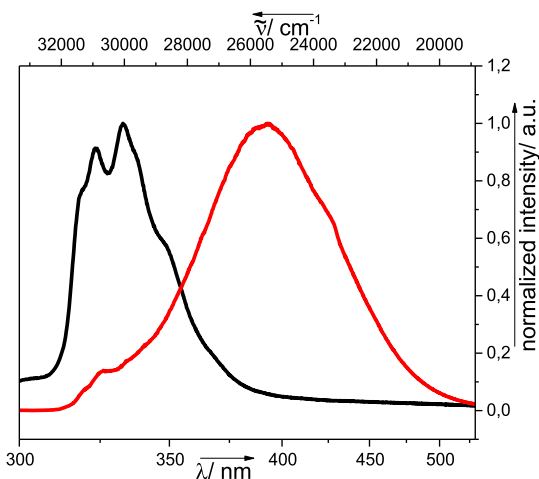


**Figure 4.** The normalized fluorescence emission spectra measured at room temperature: the MeNp aqueous solution (black line) and the pure MeNp (red line).

assigned to an excimer representing the averaged interactions in the liquid state.<sup>72</sup> A closer look, however, reveals the presence of monomer-like emission at around 325 nm and a shoulder at 430 nm. Contrariwise, the MeNp solution at 300 K exhibits emission maxima in the region of 315–360 nm, correspondingly to the monomer spectrum (Figure 4, black line)<sup>72</sup> The spectrum of the fast-cooled pure MeNp is shown in Figures 5 and S9, and the spectra of the slow-cooled sample are represented in Figure S10. In both cases, the measurements were performed after 1 h of tempering, in the range between 77 and 273 K. Both samples exhibited vibrationally resolved bands in the region from 315 to 365 nm at temperatures below 238 K; such a scenario is typical of the crystal-like structure

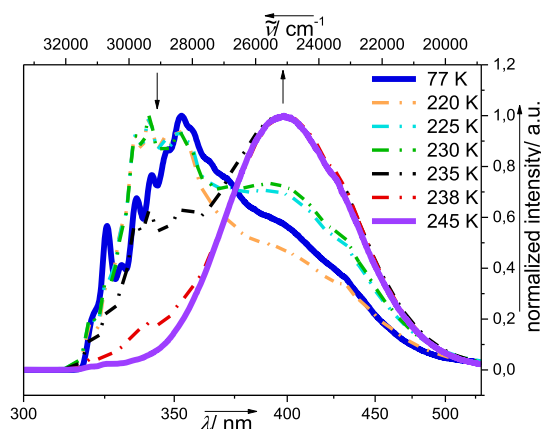


**Figure 5.** The normalized fluorescence emission spectra of the fast-cooled pure MeNp: measured at 77 K (blue solid line) and during gradual warming at 220 K (orange dash-dotted line), 225 K (cyan dash-dotted line), 230 K (green dash-dotted line), 235 K (black dash-dotted line), 238 K (red dash-dotted line), and 245 K (purple solid line).

(Figures 5, S9 and S10). At temperatures above 240 K, we detected mainly the broad band ranging from 355 to 490 nm, which corresponds to the excimer (Figures 5 and S9/S10). Below 240 K, the signal of the excimer is still traceable, but the emission signal of the crystals appears to progressively gain importance. The decreasing trend in the crystal-like signal and, conversely, the increase in the excimer emission signals are indicated by the arrows in Figure 5. The temperature at which the fluorescence signals of the crystals meet those of the excimer emission is 235 K; such a value corresponds to the melting point of the MeNp, in agreement with the DSC heating curves (Figure S8B). Moreover, we noticed that the excimer emission maximum is temperature-dependent: Below 220 K, it peaks at 400 nm, but above this temperature, the maximum is hypsochromically shifted, reaching 390 nm at 273 K. The temperature dependence of the excimer maxima is shown in Figure 6A. The shoulder at 430 nm is well-detectable at all of the measured temperatures and does not exhibit any shift of the maxima; its relative intensity increases with decreasing temperature.

**1-Methylnaphthalene Frozen Solutions.** The fluorescence emission spectra of the frozen MeNp solution measured at temperatures from 77 to 253 K and 253 to 77 K in the fast-cooled (Figure 7) and slowly-cooled variants (Figure S11), respectively, exhibited emission having a broad excimeric band with the maxima in the range of 385 and 401 nm. The excimer maxima seem to be a function of temperature, not of cooling rate, as can be deduced from a comparison of the full and empty symbols in Figure 6B. The spectra measured at 300 K exhibit monomer emission at 333 nm, as already discussed (and represented in Figure 4).

The samples of the MeNp solution were evaluated using DSC (Figure S12) to yield findings similar to those characterizing the Np solutions: an exotherm for the bulk solution crystallization at  $t = -12$  °C ( $T = 261$  K, blue line) and an endotherm for the ice melting. Again, the independent DSC analyses showed small thermal effects, stochastic in nature and appearing in the temperature range of −30 to −60 °C; these effects are possibly associated with the FCS.

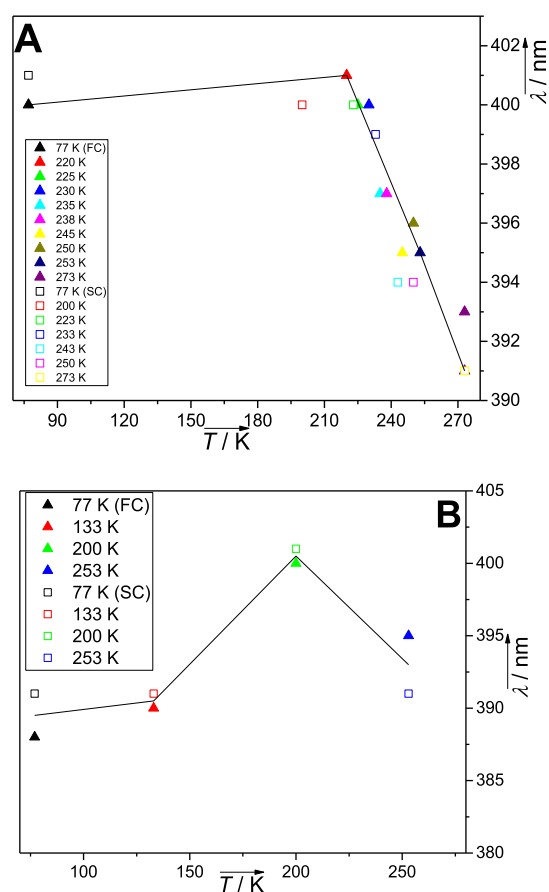


**Figure 6.** The temperature dependence of the excimer maximum wavelength in the pure MeNp (A) and the MeNp aqueous solution (B). The samples' temperatures and preparation methods (FC—fast cooling and SC—slow cooling) are indicated in the legend. The maxima are estimated from the 2nd and 4th derivation of the emission spectra. The line connecting the averages is the guide for the eyes.

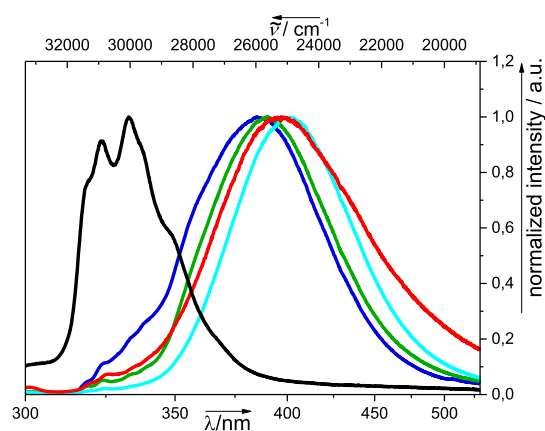


**Figure 7.** The normalized fluorescence emission spectra of the fast-cooled MeNp aqueous solution measured at 77 K (blue line), 133 K (green line), 200 K (cyan line), and 253 K (red line), and the solution spectrum at 300 K (black line).

## DISCUSSION

The room temperature fluorescence emission spectra of the Np crystals as compared to those of the aqueous solution are distinguished primarily by the slightly narrower vibrational progression peaks of the  $S_1$ – $S_0$  transition and strong self-

absorption on the blue edges of the spectra (Figures 1 and S3).<sup>73</sup> The amount of reabsorbed light directly corresponds to the thickness of the crystals, as is observed in Figure S1 and S2 and well documented in the literature.<sup>67,68</sup> The pure MeNp is a liquid at room temperature and shows mainly excimer-like emission in the fluorescence spectrum (Figure 4).<sup>73</sup> A part of the spectra of the pure MeNp appear like monomer emission (around 325 nm), and there is also a shoulder at around 430 nm, indicating other possible excimer structures.<sup>74</sup> This signal is higher in energy than the phosphorescence signal of the MeNp (471 nm) or the Np (469 nm).<sup>47,75</sup> These spectral features probably do not originate from the impurity, as they are absent from the spectra of the (frozen) solutions. The particular excimer structures were proposed by Gupta *et al.*,<sup>74</sup> based on observation of two distinct lifetimes in polymeric matrices.<sup>76,77</sup> The presence of the methyl group on the aromatic ring reduces the symmetry of the molecule, allowing multiple mutual orientations in the dimeric structures, which could explain the dual-fluorescence bands. The X-ray investigation of the liquid MeNp does not exclude such a possibility.<sup>78</sup> In certain aspects, the behavior of the liquid MeNp may resemble that of pure benzene, where already the first solvation shell shows two subpopulations differing in terms of the angle of the interaction with the closest neighbor.<sup>79,80</sup> By contrast, the emission of the MeNp aqueous solution takes the form of solvent-separated molecules, with the vibrational structure smeared out even more than that in the Np aqueous solution.

The fluorescence emission spectra in the frozen aqueous solution of the Np and the MeNp show significant differences not only between each other but also from the corresponding nonaqueous pure states. Here, we compare the spectra with those previously reported in the literature to learn about the interactions in the FCS.

The spectra of the fast-frozen and slowly frozen Np aqueous samples (Figures 2, 3, S5, and S6) are characterized by broadening on the red side of the monomer emission (350–375 nm). This property stands in contrast to solutions of nonpolar solvents at high concentrations or an ethanol solution at a low temperature, which allows for excimers with a well-developed  $\pi$ – $\pi$  overlap; the scenario then results in a distinct excimer emission having large bathochromic shifts around 385–410 nm.<sup>81,82</sup> A similar excimer emission peaking at around 400 nm is observed in layers of amorphous Np deposited on either gold<sup>83</sup> or ice<sup>48</sup> at temperatures below 77 K. Excimers are known as stabilized dimers of one excited- and one ground-state molecule, with dissociative ground-state interactions. Conversely, the presence of a second excimer, stabilized in both the ground and excited states, is typical of constrained media with restricted molecular mobility.<sup>84,85</sup> In this context, for example, the adsorption of Np on the surface of silica gel produces a second excimer emission at 375 nm,<sup>86</sup> a second excimer is also observed in polyvinyl-naphthalene glass.<sup>74,87</sup> Np-doped amorphous silica glasses show the second excimer peaking at around 380 nm at 0.5 mol/L.<sup>77,88</sup> Thus, the similarity between the Np emission spectra in the FCS and the amorphous silica glasses is indicative of the FCS being glassy, with a concentration of at least 0.5 M. As shown below, the thermal dependence of the fast-frozen samples' luminescence confirms this hypothesis even further.

We already reported broadened emission spectra interpreted as a second excimer in frozen aqueous solutions of benzene and naphthalene.<sup>46,47</sup> Here, we discuss an increase in the width

of the fluorescence emission spectrum of a fast-cooled Np solution, an effect appearing and gaining prominence during heating above approx. 150 K (see the arrow in Figures 2 and SSE). The broadening reaches its maximum at 253 K, with no significant changes above this level (Figure S5B,E). We subtracted the RT solution spectrum from the spectra of the fast-frozen solution individually measured at 77 and 253 K (Figure S13). The relevant figure demonstrates the temperature behavior of the 360 nm emission, which intensifies with increasing temperature in the ice. The negative peak with the maximum at 325 nm cannot be interpreted as an absence of the monomer emission because the crystal spectra are temperature-dependent and the self-absorption is to be expected in the frozen state; furthermore, the spectra were normalized before the subtraction. For the slowly cooled samples, analogous subtraction of the RT solution spectrum from that of the frozen solution at 253 K shows a band of similar characteristics, with the exception of the temperature evolution (Figure S14).

In the fast-frozen samples, the FCS at 77 K locks the Np molecules in conformations that do not allow full stabilization and thus manifests itself by the emission spectra being only slightly shifted from those of the monomer (a second excimer with the emission maximum at around 360 nm). At higher temperatures, a decrease in the FCS viscosity is to be expected, leading to the molecular mobility, allowing for a more pronounced signal of the second excimer because of the stronger interactions realized at higher temperatures. The broadened second excimer signal can originate from either an increased number of molecules forming it or changed spectra in the modified second excimers; based on the observed luminescence reversibility as a function of temperature, we propose that the latter suggestion embodies the correct option. If the molecules are free to diffuse within the FCS at increased temperatures, we could expect them to aggregate and to remain in such a conformation when cooled down. Thus, the spectrum should stay broadened after a warming–cooling cycle with pronounced hysteresis; however, we did not observe this effect. In this context, the fact that the spectra constitute a function of temperature and not thermal history suggests that the existing interactions between the Np molecules are more stabilizing at higher temperatures as compared to lower ones. The higher stabilization (stronger molecular stacking) was proposed to cause a bathochromic shift of the excimer emission spectra.<sup>49</sup>

A recent computational study compared the Np dimer geometries in the ground and excited states, showing that the parallel structures differ but the T-shaped ones remain similar.<sup>89</sup> The dimer with an exact face-to-face structure showed the largest stabilization in the excited state but, surprisingly, no stabilization in the ground state. The most stable ground-state geometry was revealed in the parallel interaction, with only a partial overlap of two Np molecules the angle of 49° between the molecular axes.

Thus, the FCS in the fast-frozen solution is interpretable as a glass of Np molecules mixed with water, where the Np molecules are frozen at 77 K but can alter slightly at higher temperatures to allow stronger stabilization. The emission gradually changes in a broad range of temperatures; the reversible process is likely to be connected to the Np-water glass viscosity changes.<sup>90</sup>

It should be considered that the luminescence spectra show the relative energy difference between the first excited and the

ground states; therefore, the hypsochromic shift of the second excimer with respect to the primary one can be caused by the stabilization of the ground-state dimer as compared to the two solvent-separated molecules. The question of the dynamic behavior after the excitation of an individual molecule is openly discussed in the literature,<sup>80,91</sup> as excimers are possible precursors for the formation of two triplet molecules; the process has come to be known as singlet fission.<sup>92,93</sup>

The character of the fast-cooled and slowly cooled frozen solutions' spectra openly points to the presence of precipitated crystals inside the veins; this claim is best documented by comparing the thin crystals' spectra with those of the frozen solutions at identical temperatures (Figures S3). The emission band at 315 nm is essentially absent at 77 K and gradually rises with increasing temperature. As the observation relates to thin crystals (Figure S2) and frozen solutions (Figures 2, 3 and S3), we are convinced that the crystals are present in the FCS. Furthermore, the 322 nm peak of the Np crystals was always larger for the slowly cooled solutions compared to the fast ones; hence, we deduced a higher amount of crystallized Np in the slowly cooled solutions. When inspecting the self-absorption at the blue edge, we can estimate the crystals' thickness to be about ten times larger than that of the crystals on the glass: the lower relative intensities at the 317 and 322 nm peaks in the frozen solution compared to those in the micrometric crystals suggest the formation of thicker crystals in the former. The thermal behavior (a lack of substantial growth in the 320 nm region) also indicates that the extent of the crystals present does not increase substantially during the aging. In this context, Figure 3 allows us to estimate the relative amounts of the crystals and the vitrified second excimers, showing that only a comparatively small area of the normalized spectrum can be ascribed to the crystals. Thus, we conclude that the vitrification accompanied by the formation of the second excimer is more extensive than the Np crystallization in both of the applied cooling procedures.

Our efforts to link the events deduced from the fluorescence spectra, namely, the veins' crystallization and glass transition, with the thermal events in the calorigrams were not successful, despite repeated attempts. The amount of the Np in the saturated aqueous solution approaches detection limits. The estimated crystallization heat (the molar crystallization enthalpy equals 18.9 kJ/mol<sup>66</sup>) is about  $1.2 \times 10^{-4}$  J in our sample, thus being too low to be reliably detected. The same argument is true of the detection of the heat capacity changes due to glass transition. Nevertheless, based on the temperature-dependent measurements of the Np solutions' fluorescence, we expect the  $T_g$ ' of the FCS to exceed 150 K, as the spectra do not change significantly below this temperature.

In the slowly frozen solutions, there are barely any emission spectrum changes in the measured temperature range; this finding can be interpreted as expressing better separation of the water from the aromatics. At any temperature, the spectra resemble those of the fast-frozen sample at 77 K. Apparently, the slow cooling yields an environment where no movement or changes in the relative orientation of the molecules are possible. To explain this behavior, we assume that the slow cooling produces a drier FCS with less water content and does not facilitate the plastic behavior, as will be outlined below. The slow cooling forms large ice crystals, and it can also produce glass which vitrifies at higher temperatures with proportionately smaller amounts of water, as deducible from the state diagram (Figure 8).

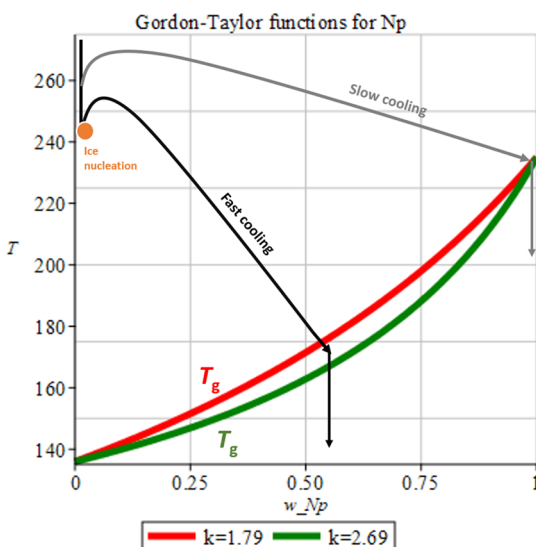


**Figure 8.** A schematic state diagram of the events in progress during the fast (black line) and the slow cooling (grey line) processes. The red and green curves are the speculative glass transition temperatures for the naphthalene solution (viz. text). After the ice nucleation begins, the release of latent crystallization heat causes the sample to warm up; the cooling rate then determines the heat dissipation rate and thus also the temperature at which the glass composition is reached (where the grey curves cross the color ones).

We would like to stress that the following paragraph is meant to demonstrate possible interpretations of the results. As the actual  $T_g'$  values for the Np are unknown, we must use rough estimates, and these may deviate markedly from the reality. Thus, the actual numerical values should be considered estimates of the orders of magnitude. As the dependence of the glass transition on the composition of the water–Np system is not known, we tried to estimate it *via* the Gordon–Taylor equation. The  $T_g$  of water is 136 K; in the NP, we estimated the  $T_g$  *via* the empirical relationship  $T_g = 2/3 T_m = 2/3 \times 353 = 235$  K.<sup>90</sup> The Gordon–Taylor equation was applied as the approximation between the  $T_g$ 's of the pure compounds, using the likely values of the linear regression-based  $k$  parameter from the paper,<sup>62</sup> Table A3 ( $k = 0.02121 \times T_g' - 2.29$ ). To obtain the  $k$  value, two  $T_g$ 's were considered: (a) 235 K, as presented above and (b) that exploiting the empirical dependence of  $T_g'$  on molecular weight, as published<sup>62</sup> (eq 3;  $M_r(\text{Np}) = 128$  g/mol gives  $T_g' = 171$  K). The method (a) yields a larger value ( $k = 2.69$ ), while the approach (b) produces a smaller one ( $k = 1.79$ ). The resulting curves that associate  $T_g'$  with varying compositions are shown in color in Figure 8. As no major change in the spectrum of the second excimer was observed below 150 K, we can set the lower limit of the  $T_g'$  to this value and the upper one to 200 K, where we positively identify an increase in the second excimer (Figure S5A). Thus, for the fast-cooled samples, the mass percentage of the Np would likely range between 0.23 (the red curve for  $k = 1.79$ ,  $T_g' = 150$  K) and 0.83 (the green curve for  $k = 2.69$ ,  $T_g' = 200$  K). This estimate corresponds to the molar concentration between 1.79 and 6.5 M, in agreement with the spectroscopic limit relating to the observation of the second excimer in the glass of the 0.5 M solution.<sup>77,88</sup> The fast- and slow-cooling processes are represented by the black and gray lines in Figure 8, respectively. The crystallization of a supercooled solution does not start later than at the homogeneous crystallization

temperature ( $T = 236$  K);<sup>94</sup> generally, we can point out that the slower the cooling process, the higher the change in the ice nucleation. This is demonstrated in Figure 8, indicating that in the slow cooling, the ice begins to crystallize at a higher temperature. The process is accompanied by a release of the latent heat warming the sample, schematically shown by a temperature increase; the heat dissipation rate depends on the cooling rate. The fast cooling in liquid nitrogen starts at a submillimolar concentration [with the  $w(\text{NP})$  close to 0]. As the cooling takes some time (ca 40 s to freeze the cuvette), the water gradually precipitates, shifting the concentration in the veins to higher values until the veins vitrify. The slow cooling leads to a much larger concentration increase, allowing the vitrification at high temperatures, as possibly corresponds to the formation of pure ice and a solution with the Np molar fraction close to 1 (7.8 M). Regrettably, the Np luminescence does not allow quantification of the freezing-induced concentration. However, we previously estimated, through analyzing the spectra of the frozen methylene blue, an increase by 3 and 6 orders of magnitude when cooling in liquid nitrogen and an ethanol bath at 253 K, respectively. As such a large growth cannot be characterized *via* the state diagram, we propose the following explanation: By the slow cooling, the FCS in the veins and on the ice surfaces allows formation of secondary ice. This assumption means that—besides the primary  $I_h$  ice that forms the ice framework and expulses the concentrated impurities into the FCS, under slow cooling and in contrast to fast cooling—microscopic ice crystals are nucleated in the FCS, making the secondary FCS even more concentrated and therefore drier and nonplastic. During the experiments, however, we did not observe a repeatable DSC signal to support this scenario, which thus remains hypothetical, despite accounting for all the observations outlined herein and presented in the relevant literature.

The fast and slow cooling of the MeNp aqueous solution (Figures 7 and S11) produced an FCS, which exhibited some differences as compared to the pure MeNp under our experimental conditions. More concretely, the amounts of crystals generated in our fast- and slow-cooling experiments are very small, and the emission band at 430 nm, sufficiently discernible in the pure MeNp (Figures 5 and S10), is not visible. Of interest is also the observed position of the excimer maxima: Regardless of the cooling rate, the maxima are temperature-dependent, with the most extreme value at about 200 K (400 nm), and they shift hypsochromically by both the cooling and the heating (Figure 6). The wavelength decrease upon cooling below 200 K stands in contrast with the behavior of the pure MeNp and is likely to be explained by the water present in the FCS. The nonobservation of difference in the fast and slow cooling of the MeNp vividly opposes the situation in the Np, possibly due to one of the following options: Either the water contents are the same or there is a difference but the mobility of the MeNp is larger than that of the Np whatever the water content may be. Regrettably, we have not performed any experiment to proceed behind the hypothesis.

**Implications for the FCS.** In the given context, we can now ask what the FCS of the studied aromatics is like. The fluorescence data of both examined compounds are strongly indicative of the prevalent formation of glass composed of a mixture of aromatics and water; in addition, the FCS contains an amount of crystals. This finding is rather surprising, as the solutions we froze approached the saturation concentrations,

making us expect a prevalence of crystals. Apparently, the formed FCS is under kinetic control and would not fully crystallize even after a week at 253 K. Contrariwise, after the sample was warmed to 253 K, the anthracene emission disappeared (Figure S5D), as the energy transfer from the Np to the anthracene did not occur anymore. Thus, the FCS was most probably restructured and separated into Np and anthracene domains. Generally, however, the FCS did not behave as being composed of the pure compounds, crystals (as in such a case, we would have expected the compound to form preferentially at low temperatures), surface-deposited compounds, or individual molecules dispersed in the ice matrix.<sup>48,95</sup> Our observations indicate more complex behavior, as the FCS clearly differs from the pure compounds; to explain this effect, the water must intermix with the aromatics. Further confirmation of the Nps' speciation differences at various ice compartments is expectable from the computational simulations.<sup>49,96–100</sup> The cooling rates caused the spectral differences in the Np, not the MeNp. Based on the temperature-dependent spectral broadening, we concluded that the Np solution is plasticized by the water when fast cooled; slow cooling does not produce such an outcome. The cooling rate has an obvious impact also on the structure of the frozen state: the resulting ice–brine morphologies can vary substantially, generating cells, dendrites, or plates,<sup>26</sup> and are understood within the models that employ temperature and concentration gradients.<sup>101–103</sup>

Supercooling, accompanied by a viscosity increase leading to the glassy state, often occurs in solutions of salts<sup>19,55</sup> and sugars.<sup>104,105</sup> In our paper, this assumption has been demonstrated for the first time in relation to nonpolar aromatic compounds. The vitrification of the FCS is facilitated by the high concentration and small vein dimensions, the latter factor allowing efficient cooling. The particular properties of the FCS are important for the chemical stability and reactivity of the compounds present. Understanding the causal dependence on the freezing rate is a matter of active research because of its direct applications in pharmaceutical stabilization, freeze casting, and others.<sup>106–109</sup>

Previously, the solution cooling rate was supposed to yield FCSs of various compositions; slower cooling would generate a glass having larger solute concentrations and lower amounts of water.<sup>36</sup> The finding is rationalized based on the relevant state diagram, where the faster cooling allows reaching the  $T_g'$  temperature with a higher water content. Thus, the faster cooling results in the FCS containing more water and vitrifying at lower temperatures; therefore, the water acts like a plasticizer.<sup>59</sup> As a matter of fact, the water in the FCS (sometimes denoted as “unfrozen water”) is a very general plasticizer,<sup>110</sup> reducing the  $T_g'$  of, for example, sugar glasses.<sup>111</sup>  $T_g'$  of ca 190 K can be estimated in a frozen solution of pyruvic acid;<sup>21</sup> the value fits in the range observed within our research, and thus, the  $T_g'$ s of various compounds can be expected to reach similar temperatures if common laboratory freezing procedures are employed.<sup>90</sup> Additionally, the presence of salts decreases the  $T_g'$  even further.<sup>60,112</sup> On the other hand, a special mechanism where the water behaves like an antiplasticizing agent is also known.<sup>113</sup>

## CONCLUSIONS

What is the FCS solution between ice crystals like during the cooling of aromatic compounds? From emission spectroscopy, we learn that the FCS forms a solution that is very

concentrated but behaves differently from the pure compounds. In the studied Np and MeNp, a portion of the FCS crystallizes but the major process rests in the formation of vitrified glasses comprising a mixture of aromatic compounds and water. The cooling rate does not have a measurable influence on the MeNp aqueous solution; however, the vitrified solution behaves distinctly in the fast- and slow-cooled Np. The fast cooling allows more molecular mobility because of the plasticizing effect of water. Overall, substantial differences in the behavior of the FCS and the pure compounds can be expected where the structural variation is only marginal; such a conclusion is applicable to both natural and anthropogenic freezing. The systems used herein are assumed to help predict the behavior and fate of aromatic hydrocarbons in cold regions.

## ASSOCIATED CONTENT

### Supporting Information

The Supporting Information is available free of charge at <https://pubs.acs.org/doi/10.1021/acs.jpbc.0c07817>.

The fluorescence emission and excitation spectra of the slow- and fast-cooled solutions and crystals measured at distinct temperatures, subtracted emission spectra, and scanning thermograms (PDF)

## AUTHOR INFORMATION

### Corresponding Author

Dominik Heger – Department of Chemistry, Faculty of Science, Masaryk University, 625 00 Brno, Czech Republic; [orcid.org/0000-0002-6881-8699](https://orcid.org/0000-0002-6881-8699); Email: [hegerd@chemi.muni.cz](mailto:hegerd@chemi.muni.cz)

### Authors

Gabriela Ondrušková – Department of Chemistry, Faculty of Science, Masaryk University, 625 00 Brno, Czech Republic  
Lukáš Veselý – Department of Chemistry, Faculty of Science, Masaryk University, 625 00 Brno, Czech Republic  
Jan Zezula – Department of Chemistry, Faculty of Science, Masaryk University, 625 00 Brno, Czech Republic  
Johannes Bachler – Institute of Physical Chemistry, University of Innsbruck, A-6020 Innsbruck, Austria  
Thomas Loerting – Institute of Physical Chemistry, University of Innsbruck, A-6020 Innsbruck, Austria; [orcid.org/0000-0001-6694-3843](https://orcid.org/0000-0001-6694-3843)

Complete contact information is available at:

<https://pubs.acs.org/10.1021/acs.jpbc.0c07817>

### Notes

The authors declare no competing financial interest.

## ACKNOWLEDGMENTS

The research was supported by Czech Science Foundation via project GA 19-08239S.

## REFERENCES

- (1) Sommerfeld, R. A. Impurities in Snowpack. *Environ. Monit. Assess.* **1989**, *12*, 66.
- (2) Bartels-Rausch, T.; et al. A review of air-ice chemical and physical interactions (AICI): liquids, quasi-liquids, and solids in snow. *Atmos. Chem. Phys.* **2014**, *14*, 1587–1633.
- (3) Shiraiwa, M.; Ammann, M.; Koop, T.; Poschl, U. Gas Uptake and Chemical Aging of Semisolid Organic Aerosol Particles. *Proc. Natl. Acad. Sci. U.S.A.* **2011**, *108*, 11003–11008.

- (4) Chakraborty, S.; Kahan, T. F. Emerging Investigator Series: Spatial Distribution of Dissolved Organic Matter in Ice and at Air-Ice Interfaces. *Environ. Sci.: Processes Impacts* **2019**, *21*, 1076–1084.
- (5) You, Y.; et al. Images reveal that atmospheric particles can undergo liquid-liquid phase separations. *Proc. Natl. Acad. Sci.* **2012**, *109*, 13188–13193.
- (6) Law, K. S.; Roiger, A.; Thomas, J. L.; Marelle, L.; Raut, J.-C.; Dalsoren, S.; Fuglestedt, J.; Tuccella, P.; Weinzierl, B.; Schlager, H. Local Arctic Air Pollution: Sources and Impacts. *Ambio* **2017**, *46*, 453–463.
- (7) Jiang, H.; Debenedetti, P. G.; Panagiotopoulos, A. Z. Nucleation in Aqueous NaCl Solutions Shifts from 1-Step to 2-Step Mechanism on Crossing the Spinodal. *J. Chem. Phys.* **2019**, *150*, 124502.
- (8) McNeill, V. F. Aqueous Organic Chemistry in the Atmosphere: Sources and Chemical Processing of Organic Aerosols. *Environ. Sci. Technol.* **2015**, *49*, 1237–1244.
- (9) Guzmán, M. I.; Hoffmann, M. R.; Colussi, A. J. Photolysis of Pyruvic Acid in Ice: Possible Relevance to Co and Co<sub>2</sub> Ice Core Record Anomalies. *J. Geophys. Res. Atmos.* **2007**, *112*, D10123.
- (10) Dong, Z.; Kang, S.; Qin, D.; Shao, Y.; Ulbrich, S.; Qin, X. Variability in individual particle structure and mixing states between the glacier-snowpack and atmosphere in the northeastern Tibetan Plateau. *Cryosphere* **2018**, *12*, 3877–3890.
- (11) McNeill, V. F.; et al. Organics in Environmental Ices: Sources, Chemistry, and Impacts. *Atmos. Chem. Phys.* **2012**, *12*, 9653–9678.
- (12) Knopf, D. A.; Alpert, P. A.; Wang, B. The Role of Organic Aerosol in Atmospheric Ice Nucleation: A Review. *ACS Earth Space Chem.* **2018**, *2*, 168–202.
- (13) Yang, X.; Neděla, V.; Runštuk, J.; Ondrušková, G.; Krausko, J.; Vetráková, L.; Heger, D. Evaporating Brine from Frost Flowers with Electron Microscopy and Implications for Atmospheric Chemistry and Sea-Salt Aerosol Formation. *Atmos. Chem. Phys.* **2017**, *17*, 6291–6303.
- (14) Wania, F. Assessing the Potential of Persistent Organic Chemicals for Long-Range Transport and Accumulation in Polar Regions. *Environ. Sci. Technol.* **2003**, *37*, 1344–1351.
- (15) Bonasoni, P.; Cristofanelli, P.; Marinoni, A.; Vuillermoz, E.; Adhikary, B. Atmospheric Pollution in the Hindu Kush-Himalaya Region. *Mt. Res. Dev.* **2012**, *32*, 468–479.
- (16) Qiu, J. *Pollutants Waft over the Himalayas*; Nature Apr 14, 2015, 2015.
- (17) Petrenko, V. F.; Whitworth, R. W. *Physics of Ice*; Oxford University Press: Oxford, 1999.
- (18) Takenaka, N.; Ueda, A.; Daimon, T.; Bandow, H.; Dohmaru, T.; Maeda, Y. Acceleration Mechanism of Chemical Reaction by Freezing: The Reaction of Nitrous Acid with Dissolved Oxygen. *J. Phys. Chem.* **1996**, *100*, 13874–13884.
- (19) Imrichová, K.; Veselý, L.; Gasser, T. M.; Loerting, T.; Neděla, V.; Heger, D. Vitrification and Increase of Basicity in between Ice Ih Crystals in Rapidly Frozen Dilute NaCl Aqueous Solutions. *J. Chem. Phys.* **2019**, *151*, 014503.
- (20) Krausková, L.; Procházková, J.; Klášková, M.; Filipová, L.; Chaloupková, R.; Malý, S.; Damborský, J.; Heger, D. Suppression of Protein Inactivation During Freezing by Minimizing pH Changes Using Ionic Cryoprotectants. *Int. J. Pharm.* **2016**, *509*, 41–49.
- (21) Guzmán, M. I.; Colussi, A. J.; Hoffmann, M. R. Photogeneration of Distant Radical Pairs in Aqueous Pyruvic Acid Glasses. *J. Phys. Chem. A* **2006**, *110*, 931–935.
- (22) Guzmán, M. I.; Hildebrandt, L.; Colussi, A. J.; Hoffmann, M. R. Cooperative Hydration of Pyruvic Acid in Ice. *J. Am. Chem. Soc.* **2006**, *128*, 10621–10624.
- (23) Hudait, A.; Molinero, V. What Determines the Ice Polymorph in Clouds? *J. Am. Chem. Soc.* **2016**, *138*, 8958–8967.
- (24) Liu, X.; Zhuang, K.; Lin, S.; Zhang, Z.; Li, X. Determination of Supercooling Degree, Nucleation and Growth Rates, and Particle Size for Ice Slurry Crystallization in Vacuum. *Crystals* **2017**, *7*, 128.
- (25) Hullar, T.; Anastasio, C. Direct Visualization of Solute Locations in Laboratory Ice Samples. *Cryosphere* **2016**, *10*, 2057–2068.
- (26) Vetráková, L.; Neděla, V.; Runštuk, J.; Heger, D. The Morphology of Ice and Liquid Brine in an Environmental Scanning Electron Microscope: A Study of the Freezing Methods. *Cryosphere* **2019**, *13*, 2385–2405.
- (27) Kiani, H.; Sun, D.-W. Water Crystallization and Its Importance to Freezing of Foods: A Review. *Trends Food Sci. Technol.* **2011**, *22*, 407–426.
- (28) Heger, D.; Jirkovský, J.; Klán, P. Aggregation of Methylene Blue in Frozen Aqueous Solutions Studied by Absorption Spectroscopy. *J. Phys. Chem. A* **2005**, *109*, 6702–6709.
- (29) Heger, D.; Klánová, J.; Klán, P. Enhanced Protonation of Cresol Red in Acidic Aqueous Solutions Caused by Freezing. *J. Phys. Chem. B* **2006**, *110*, 1277–1287.
- (30) Bogdan, A.; Molina, M. J.; Tenhu, H.; Bertel, E.; Bogdan, N.; Loerting, T. Visualization of Freezing Process in Situ Upon Cooling and Warming of Aqueous Solutions. *Sci. Rep.* **2014**, *4*, 7414.
- (31) O'Concubhair, R.; Sodeau, J. R. The Effect of Freezing on Reactions with Environmental Impact. *Acc. Chem. Res.* **2013**, *46*, 2716–2724.
- (32) Inagawa, A.; Ishikawa, T.; Kusunoki, T.; Ishizaka, S.; Harada, M.; Otsuka, T.; Okada, T. Viscosity of Freeze-Concentrated Solution Confined in Micro/Nanospace Surrounded by Ice. *J. Phys. Chem. C* **2017**, *121*, 12321–12328.
- (33) Vetráková, L.; Neděla, V.; Runštuk, J.; Tihlaříková, E.; Heger, D.; Shalae, E. Dynamical in-Situ Observation of the Lyophilization and Vacuum-Drying Processes of a Model Biopharmaceutical System by an Environmental Scanning Electron Microscope. *Int. J. Pharm.* **2020**, *585*, 119448.
- (34) Krausko, J.; Runštuk, J.; Neděla, V.; Klán, P.; Heger, D. Observation of a Brine Layer on an Ice Surface with an Environmental Scanning Electron Microscope at Higher Pressures and Temperatures. *Langmuir* **2014**, *30*, 5441–5447.
- (35) Kulikov, M.; Feigin, A.; Schrems, O. H<sub>2</sub>O<sub>2</sub> Photoproduction inside H<sub>2</sub>O and H<sub>2</sub>O:O<sub>2</sub> Ices at 20–140 K. *Sci. Rep.* **2019**, *9*, 11375.
- (36) MacFarlane, D. R. Physical Aspects of Vitrification in Aqueous Solutions. *Cryobiology* **1987**, *24*, 181–195.
- (37) Zhang, Y.; et al. The Cooling Rate- and Volatility-Dependent Glass-Forming Properties of Organic Aerosols Measured by Broadband Dielectric Spectroscopy. *Environ. Sci. Technol.* **2019**, *53*, 12366–12378.
- (38) Vetráková, L.; Neděla, V.; Runštuk, J.; Tihlaříková, E.; Heger, D.; Shalae, E. Dynamical in-Situ Observation of the Lyophilization and Vacuum-Drying Processes of a Model Biopharmaceutical System by an Environmental Scanning Electron Microscope. *Int. J. Pharm.* **2020**, *585*, 119448.
- (39) Zhang, Y.; Tao, S. Global Atmospheric Emission Inventory of Polycyclic Aromatic Hydrocarbons (PAHs) for 2004. *Atmos. Environ.* **2009**, *43*, 812–819.
- (40) Ellickson, K. M.; McMahon, C. M.; Herbrandson, C.; Krause, M. J.; Schmitt, C. M.; Lippert, C. J.; Pratt, G. C. Analysis of Polycyclic Aromatic Hydrocarbons (PAHs) in Air Using Passive Sampling Calibrated with Active Measurements. *Environ. Pollut.* **2017**, *231*, 487–496.
- (41) Sun, C.; Zhang, J.; Ma, Q.; Chen, Y.; Ju, H. Polycyclic Aromatic Hydrocarbons (PAHs) in Water and Sediment from a River Basin: Sediment-Water Partitioning, Source Identification and Environmental Health Risk Assessment. *Environ. Geochem. Health* **2017**, *39*, 63–74.
- (42) Szolar, O. H. J.; Rost, H.; Braun, R.; Loibner, A. P. Analysis of Polycyclic Aromatic Hydrocarbons in Soil: Minimizing Sample Pretreatment Using Automated Soxhlet with Ethyl Acetate as Extraction Solvent. *Anal. Chem.* **2002**, *74*, 2379–2385.
- (43) Salama, F. PAHs in Astronomy - A Review. *Proc. Int. Astron. Union* **2008**, *4*, 357–366.
- (44) Perkampus, H. H. *UV-Vis Atlas of Organic Compounds*; VCH, 1992.
- (45) Heger, D.; Klán, P. Interactions of Organic Molecules at Grain Boundaries in Ice: A Solvatochromic Analysis. *J. Photochem. Photobiol., A* **2007**, *187*, 275–284.

- (46) Kania, R.; Malongwe, J. K. E.; Nachtigallová, D.; Krausko, J.; Gladich, I.; Roeselová, M.; Heger, D.; Klán, P. Spectroscopic Properties of Benzene at the Air-Ice Interface: A Combined Experimental-Computational Approach. *J. Phys. Chem. A* **2014**, *118*, 7535–7547.
- (47) Krausko, J.; Malongwe, J. K. E.; Bičanová, G.; Klán, P.; Nachtigallová, D.; Heger, D. Spectroscopic Properties of Naphthalene on the Surface of Ice Grains Revisited: A Combined Experimental-Computational Approach. *J. Phys. Chem. A* **2015**, *119*, 8565–8578.
- (48) Ondrušková, G.; Krausko, J.; Stern, J. N.; Hauptmann, A.; Loerting, T.; Heger, D. Distinct Speciation of Naphthalene Vapor Deposited on Ice Surfaces at 253 or 77 K: Formation of Submicrometer-Sized Crystals or an Amorphous Layer. *J. Phys. Chem. C* **2018**, *122*, 11945–11953.
- (49) Heger, D.; Nachtigallová, D.; Surman, F.; Krausko, J.; Magyarová, B.; Brumovský, M.; Rubeš, M.; Gladich, I.; Klán, P. Self-Organization of 1-Methylnaphthalene on the Surface of Artificial Snow Grains: A Combined Experimental-Computational Approach. *J. Phys. Chem. A* **2011**, *115*, 11412–11422.
- (50) Krausko, J.; Ondrušková, G.; Heger, D. Comment on “Photolysis of Polycyclic Aromatic Hydrocarbons on Water and Ice Surfaces” and on “Nonchromophoric Organic Matter Suppresses Polycyclic Aromatic Hydrocarbon Photolysis in Ice and at Ice Surfaces”. *J. Phys. Chem. A* **2015**, *119*, 10761–10763.
- (51) Charnawskas, J. C.; et al. Condensed-Phase Biogenic-Anthropogenic Interactions with Implications for Cold Cloud Formation. *Faraday Discuss.* **2017**, *200*, 165–194.
- (52) Wang, B.; Lambe, A. T.; Massoli, P.; Onasch, T. B.; Davidovits, P.; Worsnop, D. R.; Knopf, D. A. The Deposition Ice Nucleation and Immersion Freezing Potential of Amorphous Secondary Organic Aerosol: Pathways for Ice and Mixed-Phase Cloud Formation. *J. Geophys. Res. Atmos.* **2012**, *117*, D16209.
- (53) Reid, J. P.; Bertram, A. K.; Topping, D. O.; Laskin, A.; Martin, S. T.; Petters, M. D.; Pope, F. D.; Rovelli, G. The Viscosity of Atmospherically Relevant Organic Particles. *Nat. Commun.* **2018**, *9*, 956.
- (54) Kohl, I.; Bachmann, L.; Mayer, E.; Hallbrucker, A.; Loerting, T. Glass transition in hyperquenched water? *Nature* **2005**, *435*, No. E1.
- (55) Bachler, J.; Handle, P. H.; Giovambattista, N.; Loerting, T. Glass Polymorphism and Liquid-Liquid Phase Transition in Aqueous Solutions: Experiments and Computer Simulations. *Phys. Chem. Chem. Phys.* **2019**, *21*, 23238–23268.
- (56) Murray, B. J.; Bertram, A. K. Inhibition of solute crystallisation in aqueous H<sup>+</sup>-NH<sub>4</sub><sup>+</sup>-SO<sub>4</sub><sup>2-</sup>-H<sub>2</sub>O droplets. *Phys. Chem. Chem. Phys.* **2008**, *10*, 3287.
- (57) Bergman, R.; Swenson, J. Dynamics of Supercooled Water in Confined Geometry. *Nature* **2000**, *403*, 283.
- (58) Zhao, L.; Pan, L.; Cao, Z.; Wang, Q. Confinement-Induced Vitrification of Aqueous Sodium Chloride Solutions. *Chem. Phys. Lett.* **2016**, *647*, 170–174.
- (59) Pikal, M. J.; Shah, S. The Collapse Temperature in Freeze Drying: Dependence on Measurement Methodology and Rate of Water Removal from the Glassy Phase. *Int. J. Pharm.* **1990**, *62*, 165–186.
- (60) Chang, B. S.; Randall, C. S. Use of Subambient Thermal Analysis to Optimize Protein Lyophilization. *Cryobiology* **1992**, *29*, 632–656.
- (61) Vetráková, L.; Vykoukal, V.; Heger, D. Comparing the Acidities of Aqueous, Frozen, and Freeze-Dried Phosphate Buffers: Is There a “Ph Memory” Effect? *Int. J. Pharm.* **2017**, *530*, 316–325.
- (62) Zobrist, B.; Marcolli, C.; Pedernera, D. A.; Koop, T. Do Atmospheric Aerosols Form Glasses? *Atmos. Chem. Phys.* **2008**, *8*, 5221–5244.
- (63) Pansare, S. K.; Patel, S. M. Practical Considerations for Determination of Glass Transition Temperature of a Maximally Freeze Concentrated Solution. *AAPS PharmSciTech* **2016**, *17*, 805–819.
- (64) Perez-Tejeda, P.; Yanes, C.; Maestre, A. Solubility of Naphthalene in Water + Alcohol Solutions at Various Temperatures. *J. Chem. Eng. Data* **1990**, *35*, 244–246.
- (65) Dickhut, R. M.; Miller, K. E.; Andren, A. W. Evaluation of Total Molecular Surface Area for Predicting Air-Water Partitioning Properties of Hydrophobic Aromatic Chemicals. *Chemosphere* **1994**, *29*, 283–297.
- (66) McCullough, J. P.; Finke, H. L.; Messerly, J. F.; Todd, S. S.; Kincheloe, T. C.; Waddington, G. The Low-Temperature Thermodynamic Properties of Naphthalene, L-Methylnaphthalene, 2-Methylnaphthalene, 1,2,3,4-Tetrahydronaphthalene, Trans-Decahydronaphthalene and Cis-Decahydronaphthalene. *J. Phys. Chem.* **1957**, *61*, 1105–1116.
- (67) Uchida, K. Reabsorption Effect and Fluorescence Decay Times in Naphthalene Crystals. *Memoirs of the Fukui Institute of Technology* **1984**, *14*, 121–125.
- (68) Ahn, T.-S.; Muller, A. M.; Al-Kaysi, R. O.; Spano, F. C.; Norton, J. E.; Beljonne, D.; Bredas, J. L.; Bardeen, C. J. Experimental and Theoretical Study of Temperature Dependent Exciton Delocalization and Relaxation in Anthracene Thin Films. *J. Chem. Phys.* **2008**, *128*, 054505.
- (69) Márquez, F.; Zicovich-Wilson, C. M.; Corma, A.; Palomares, E.; García, H. Naphthalene Included within All-Silica Zeolites: Influence of the Host on the Naphthalene Photophysics. *J. Phys. Chem. B* **2001**, *105*, 9973–9979.
- (70) Auweter, H.; Braun, A.; Mayer, U.; Schmid, D. Dynamics of Energy Transfer by Singlet Excitons in Naphthalene Crystals as Studied by Time-Resolved Spectroscopy. *Z. Naturforsch., A: Phys. Sci.* **1979**, *34*, 761–772.
- (71) Yokoyama, C.; Ebina, T.; Takahashi, S. Melting Temperatures of Several Polycyclic and Heteropolycyclic Aromatic Compounds under High Pressures. *Fluid Phase Equilib.* **1993**, *84*, 207–223.
- (72) Mataga, N.; Tomura, M.; Nishimura, H. Fluorescence Decay Times of Naphthalene and Naphthalene Excimers. *Mol. Phys.* **1965**, *9*, 367–375.
- (73) Kawakubo, T. On the Emission of Naphthalene and Some of Its Derivatives in the Crystalline State. *Mol. Cryst. Liq. Cryst.* **1972**, *16*, 333–353.
- (74) Gupta, A.; Liang, R.; Moacanin, J.; Kliger, D.; Goldbeck, R.; Horwitz, J.; Miskowski, V. M. Internal conversion in poly(1-vinylnaphthalene)-IV. Photochemical processes in polymeric systems. *Eur. Polym. J.* **1981**, *17*, 485–490.
- (75) Terenin, A.; Ermolaev, V. Sensitized Phosphorescence in Organic Solutions at Low Temperature. Energy Transfer between Triplet States. *Trans. Faraday Soc.* **1956**, *52*, 1042–1052.
- (76) Holden, D. A.; Corey, L.; Kovarova, J.; Guillet, J. E. Effects of Chromophore Environment on the Photophysics of Poly(2-Isopropenylnaphthalene). *Macromolecules* **1986**, *19*, 1180–1186.
- (77) Kitamura, T.; Takahashi, Y.; Yamanaka, T.; Uchida, K. Luminescence Associated with the Molecular Aggregation of Hydrocarbons Doped in Amorphous Silica Glasses. *J. Lumin.* **1991**, *48–49*, 373–376.
- (78) Drozdowski, H. Local Structure and Molecular Correlations in Liquid 1-Methylnaphthalene at 293 K. *Chem. Phys. Lett.* **2002**, *351*, 53–60.
- (79) Headen, T. F.; Howard, C. A.; Skipper, N. T.; Wilkinson, M. A.; Bowron, D. T.; Soper, A. K. Structure of  $\pi$ - $\pi$  Interactions in Aromatic Liquids. *J. Am. Chem. Soc.* **2010**, *132*, 5735–5742.
- (80) Iyer, E. S. S.; Sadybekov, A.; Lioubashevski, O.; Krylov, A. I.; Ruhman, S. Rewriting the Story of Excimer Formation in Liquid Benzene. *J. Phys. Chem. A* **2017**, *121*, 1962–1975.
- (81) Förster, T. Excimers. *Angew. Chem., Int. Ed.* **1969**, *8*, 333–343.
- (82) Parker, C. A. Delayed Fluorescence from Naphthalene Solutions. *Spectrochim. Acta* **1963**, *19*, 989–994.
- (83) Nakayama, H.; Hosokawa, T.; Ishii, K. Fluorescence Spectra and Energy Transfer in Amorphous Naphthalene. *Chem. Phys. Lett.* **1998**, *289*, 275–280.

- (84) Barashkov, N. N.; Sakhno, T. V.; Nurmukhametov, R. N.; Khakhel, O. A. Excimers of Organic Molecules. *Usp. Khim.* **1993**, *62*, 539–552.
- (85) Birks, J. B. Excimers. *Rep. Prog. Phys.* **1975**, *38*, 903–974.
- (86) Hara, K.; De Mayo, P.; Ware, W. R.; Weedon, A. C.; Wong, G. S. K.; Wu, K. C. Biphasic photochemistry: time-resolved spectra of adsorbed hydrocarbons. *Chem. Phys. Lett.* **1980**, *69*, 105–108.
- (87) Nakahira, T.; Ishizuka, S.; Iwabuchi, S.; Kojima, K. “Second Excimer” Luminescence from Polymers with Sterically Hindered Naphthalene Chromophores. *Macromolecules* **1982**, *15*, 1217–1218.
- (88) Yamanaka, T.; Takahashi, Y.; Uchida, K. Time-Resolved Fluorescence Spectra of Naphthalene Doped in Amorphous Silica Glasses. *Chem. Phys. Lett.* **1990**, *172*, 405–408.
- (89) Dubinets, N. O.; Safonov, A. A.; Bagaturyants, A. A. Structures and Binding Energies of the Naphthalene Dimer in Its Ground and Excited States. *J. Phys. Chem. A* **2016**, *120*, 2779–2782.
- (90) Angell, C. A. Liquid Fragility and the Glass Transition in Water and Aqueous Solutions. *Chem. Rev.* **2002**, *102*, 2627–2650.
- (91) Hoche, J.; Schmitt, H.-C.; Humeniuk, A.; Fischer, I.; Mitrić, R.; Röhr, M. I. S. The Mechanism of Excimer Formation: An Experimental and Theoretical Study on the Pyrene Dimer. *Phys. Chem. Chem. Phys.* **2017**, *19*, 25002–25015.
- (92) Wilson, M. W. B.; Rao, A.; Ehrler, B.; Friend, R. H. Singlet Exciton Fission in Polycrystalline Pentacene: From Photophysics toward Devices. *Acc. Chem. Res.* **2013**, *46*, 1330–1338.
- (93) Smith, M. B.; Michl, J. Recent Advances in Singlet Fission. In *Annual Review of Physical Chemistry*; Johnson, M. A., Martinez, T. J., Eds.; Annual Reviews: Palo Alto, 2013; Vol. 64, pp 361–386.
- (94) Tanaka, K. K.; Kimura, Y. Theoretical Analysis of Crystallization by Homogeneous Nucleation of Water Droplets. *Phys. Chem. Chem. Phys.* **2019**, *21*, 2410–2418.
- (95) Lignell, A.; Gudipati, M. S. Mixing of the Immiscible: Hydrocarbons in Water-Ice near the Ice Crystallization Temperature. *J. Phys. Chem. A* **2015**, *119*, 2607–2613.
- (96) Michoulier, E.; Ben Amor, N.; Rapacioli, M.; Noble, J. A.; Mascetti, J.; Toubin, C.; Simon, A. Theoretical Determination of Adsorption and Ionisation Energies of Polycyclic Aromatic Hydrocarbons on Water Ice. *Phys. Chem. Chem. Phys.* **2018**, *20*, 11941–11953.
- (97) Mészár, Z. E.; Hantal, G.; Picaud, S.; Jedlovsky, P. Adsorption of Aromatic Hydrocarbon Molecules at the Surface of Ice, as Seen by Grand Canonical Monte Carlo Simulation. *J. Phys. Chem. C* **2013**, *117*, 6719–6729.
- (98) Hudait, A.; Allen, M. T.; Molinero, V. Sink or Swim: Ions and Organics at the Ice-Air Interface. *J. Am. Chem. Soc.* **2017**, *139*, 10095–10103.
- (99) Liyana-Arachchi, T. P.; Valsaraj, K. T.; Hung, F. R. Ice Growth from Supercooled Aqueous Solutions of Reactive Oxygen Species. *Theor. Chem. Accounts* **2013**, *132*, 1309.
- (100) Liyana-Arachchi, T. P.; Valsaraj, K. T.; Hung, F. R. Adsorption of Naphthalene and Ozone on Atmospheric Air/Ice Interfaces Coated with Surfactants: A Molecular Simulation Study. *J. Phys. Chem. A* **2012**, *116*, 2519–2528.
- (101) Maus, S. Prediction of the Cellular Microstructure of Sea Ice by Morphological Stability Theory. *Physics and Chemistry of Ice*; Kuhs, W. F., Ed.; Royal Society of Chemistry, 2007; pp 371–382.
- (102) Rohatgi, P. K.; Adams, C. M. Ice-Brine Dendritic Aggregate formed on Freezing of Aqueous Solutions. *J. Glaciol.* **1967**, *6*, 663–679.
- (103) Wettlaufer, J. S. Directional Solidification of Salt Water: Deep and Shallow Cells. *Europhys. Lett.* **1992**, *19*, 337–342.
- (104) Longinotti, M. P.; Corti, H. R. Viscosity of Concentrated Sucrose and Trehalose Aqueous Solutions Including the Supercooled Regime. *J. Phys. Chem. Ref. Data* **2008**, *37*, 1503–1515.
- (105) Ollett, A.-L.; Parker, R. The Viscosity of Supercooled Fructose and Its Glass Transition Temperature. *J. Texture Stud.* **1990**, *21*, 355–362.
- (106) Hauptmann, A.; Podgoršek, K.; Kuzman, D.; Srčić, S.; Hoelzl, G.; Loerting, T. Impact of Buffer, Protein Concentration and Sucrose Addition on the Aggregation and Particle Formation During Freezing and Thawing. *Pharmaceut. Res.* **2018**, *35*, 101.
- (107) Schremp, M.; Campbell, J. M.; Christenson, H. K.; Tropea, C. Ice Layer Spreading Along a Solid Substrate During Solidification of Supercooled Water: Experiments and Modeling. *Langmuir* **2017**, *33*, 4870–4877.
- (108) Schremp, M.; Tropea, C. Solidification of Supercooled Water in the Vicinity of a Solid Wall. *Phys. Rev. E* **2016**, *94*, 052804.
- (109) Dedovets, D.; Monteux, C.; Deville, S. Five-Dimensional Imaging of Freezing Emulsions with Solute Effects. *Science* **2018**, *360*, 303–306.
- (110) Matveev, Y.; Grinberg, V. Y.; Tolstoguzov, V. B. The Plasticizing Effect of Water on Proteins, Polysaccharides and Their Mixtures. Glassy State of Biopolymers, Food and Seeds. *Food Hydrocolloids* **2000**, *14*, 425–437.
- (111) Tonniss, W. F.; Mensink, M. A.; de Jager, A.; van der Voort Maarschalk, K.; Frijlink, H. W.; Hinrichs, W. L. J. Size and Molecular Flexibility of Sugars Determine the Storage Stability of Freeze-Dried Proteins. *Mol. Pharm.* **2015**, *12*, 684–694.
- (112) Nesarikar, V. V.; Nassar, M. N. Effect of Cations and Anions on Glass Transition Temperatures in Excipient Solutions. *Pharm. Dev. Technol.* **2007**, *12*, 259–264.
- (113) Ruiz, G. N.; Romanini, M.; Hauptmann, A.; Loerting, T.; Shalae, E.; Tamarit, J. L.; Pardo, L. C.; Macovez, R. Genuine Antiplasticizing Effect of Water on a Glass-Former Drug. *Sci. Rep.* **2017**, *7*, 7470.